Sedimentology (2009) **56,** 421–438 doi: 10.1111/j.1365-3091.2008.00977.x

Grain-size information from the statistical properties of digital images of sediment

DANIEL BUSCOMBE and GERHARD MASSELINK
School of Geography, University of Plymouth, Plymouth PL4 8AA, UK
(E-mail: daniel.buscombe@plymouth.ac.uk; gerd.masselink@plymouth.ac.uk)

Associate Editor: Susan Marriott

ABSTRACT

The autocorrelation technique for estimating grain-size from digital images of sand beds has been extended and validated for use on coarse sand (0·7 mm) and gravel (up to ~20 mm). A number of aspects of the technique have been explored and some potential improvements suggested. Autocorrelation is just one suitable statistical method sensitive to the grain-size of sediment in digital images; four additional techniques are presented and their relative merits discussed. A collective suite of techniques applicable to the general problem of grain-size estimation from digital images of sediment might broaden the applicability to more sedimentary environments, as well as improve its accuracy. These techniques are compared using a large data set from a gravel barrier beach in southern England. Based on over 180 samples, mean grain-size of sieved and imaged sediments correspond to within between 8% and 16%. Some theoretical aspects of the spatial arrangement of image intensity in digital images of natural sediments are addressed, including the fractal nature of sediments in images, which has potential implications for derivation of grain-size distributions from images of sand-sized material through segmentation and thresholding. The methods outlined in this contribution may also find application in further uncovering the geometric structure of sediment beds, as well as in the simulation of sedimentation processes.

Keywords Grain size analysis, digital images, statistical models, gravel beach.

INTRODUCTION

Grain-size information from natural environments traditionally is obtained using methods such as sieving, laser diffraction and settling, which do not help measure equivalent properties of the sample. In addition, the slow and labour-intensive nature of these methodologies has limited the spatial and temporal resolution at which grain-size data are obtained. Where grain-size is an important parameter, such as in determining sediment transport, studies can be limited fundamentally by the difficulty in sampling for sediment at the required frequency. A further disadvantage is that sediment must be removed from the natural environment, potentially altering subsequent system development. In contrast, photographic methods can be used to measure sediment size at a resolution comparable with measurements of hydraulic, hydrodynamic and morphological/topographical conditions without disrupting the sediment body by direct sampling.

The problem of deriving sediment size information from digital images of sediment has been approached using two different families of techniques. The first is based on edge detection and image segmentation principles (e.g. Butler *et al.*, 2001; Sime & Ferguson, 2003; Graham *et al.*, 2005). Such techniques rely on marked image-intensity contrasts between grains and gaps between grains (interstices), such that thresholds can be specified to discriminate individual grains from the background intensity levels (e.g. Sime & Ferguson, 2003). Thus far, these methods are

suitable only in instances where the overlapping of individual grains, or the apparent coalescence of adjacent grains because of indistinguishable similarities in colour and texture, are negligible. Such images are much more likely to be found in the larger sediment fractions, such as coarse gravels or surfaces composed of distinctive bimodal mixtures (e.g. clay matrix and gravel framework), where thresholds can be applied to remove entire classes of grains. More usually, images of samples of natural sediments are comprised of complicated objects that are difficult to segment. Specifically, they have a greater number of individual grains per image (Fig. 1) and so the potential for errors associated with grain overlap and grain coalescence is significant.

The second approach is to treat grains within an image not as individual objects, but as a collection of 'textures'. With reference to Fig. 1, sediments of varying sizes have recognizably different textures, for example the spatial arrangement of greyscale intensities is much more variable in images of smaller sediment sizes (Fig. 1). In such cases, accurate grain-size information of natural sediment surfaces may be derived through the statistical properties of those images, based on the notion that intensity values in any cross-section of digital images of sediment (Fig. 1) are more similar over space in coarse sediments than in fine sediments. This type of work stems from Rubin (2004), which proposed an autocorrelation algorithm for use on sand-sized sediment. Its utility for derivation of mean grain-size has been demonstrated and validated by Rubin *et al.* (2006, 2007) and Barnard *et al.* (2007), and it has been used in a range of sedimentary environments (e.g. Gallagher *et al.*, 2006; Austin & Bullard, 2007; Ruggiero *et al.*, 2007). Similar ideas have been developed for characterizing large-scale sediment patches from aerial photography (e.g. Carbonneau *et al.*, 2004, 2005).

This contribution extends the statistical approach in two ways. Firstly, by designing and validating a field image-collection methodology for use with gravel-sized sediment. Secondly, and more importantly, the general problem of obtaining an estimate of grain-size from an image of sand/gravel is put on a firmer theoretical basis by

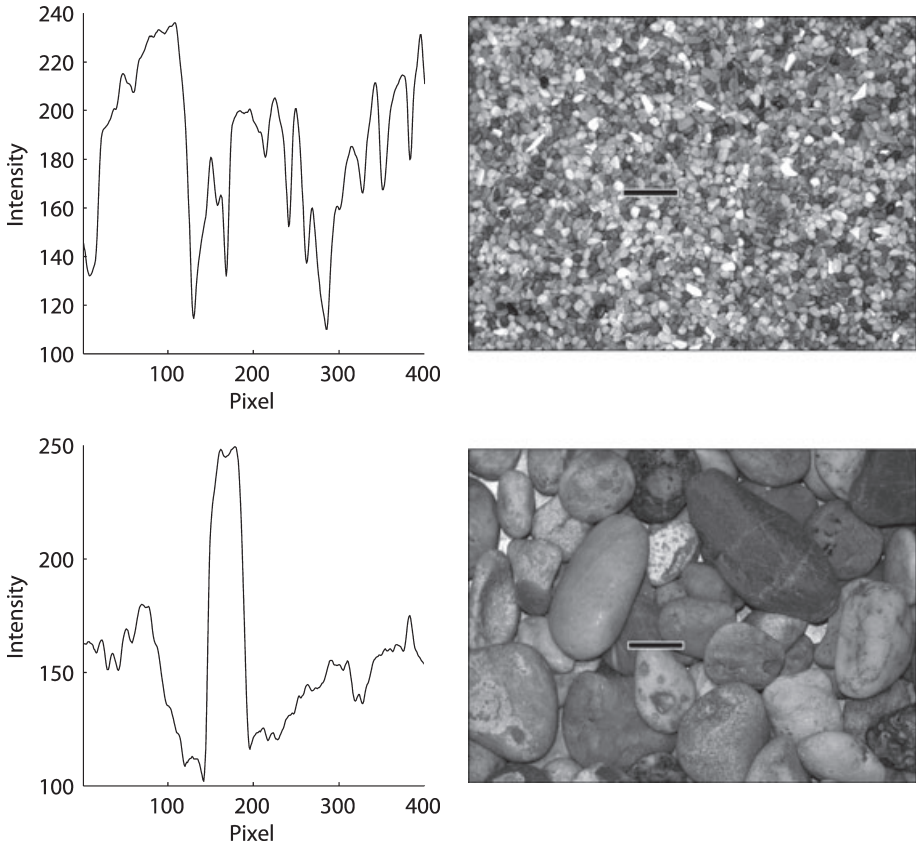

Fig. 1. The nature of intensity variations in images of sediment. Left panels: cross-sectional profile through images of 2 and 16 mm sediment. Right panels: the corresponding images, with example scale-bar for the intensity traces on the left.

extending the theoretical/algorithmic work of Rubin (2004).

The structure of the paper is as follows. After a detailed introduction to the general problem of obtaining an estimate of grain-size from a digital image of sediment, termed 'look-up cataloguing' (LUC), four new numerical methods are introduced, three of which are prompted by the suggestion that the two-dimensional (fast) Fourier transform (hereafter referred to as '2D-FT') may be a viable alternative to the spatial autocorrelation routine to derive grain-size information from digital images of natural mixed beds (Rubin, 2004). The 2D-FT algorithm has been applied to images for derivation of variograms, power spectra and fractal dimensions. The fourth numerical procedure is an autoregressive model, which quantifies serial correlation and thus is in the same family of methods as the autocorrelation function. It is found that similar results are achieved using a number of different numerical techniques. Some example research applications are presented from a gravel beach, and the relative merits of different methods to obtain grain-size from images of sediment are evaluated. Theoretical considerations of the LUC approach, as well as the use of both statistical and segmentation methods in practice, are discussed before conclusions are drawn.

Several techniques have been utilized firstly because this approach allows the nature of spatial variability of grey-level intensities within images of sediment to be explored theoretically. It may, therefore, provide a starting point to the rapid, automated and quantitative description of additional sedimentological traits such as grain orientation, shape, sorting, bimodality and mineralogy, which should be possible using the techniques presented in this paper for sizing. In addition, the use of these techniques may be useful in artificially modelling grain surfaces for use in sediment transport simulations and elsewhere. Researchers working in a wide range of environments are more accustomed to certain techniques than others, so the adoption of statistical sedimentological techniques is facilitated by exploring and suggesting a range of acceptable alternatives. Finally, as at present the primary advantage of LUC methods for sediment size is sample processing speed, a number of methods have been suggested, the speed or accuracy of which may depend on the software or (high-level) programming language used.

DIGITAL GRAIN-SIZE METHODOLOGY

Overview of sedimentary LUC

A standard red–green–blue (RGB) digital image is transformed into a greyscale (intensity) image by eliminating the hue and saturation information, while retaining the luminance. The resulting 2D matrix is composed of 8 bit values, which score shades of grey (intensity) in the visible spectrum on a 0:255 point scale. Figure 1 demonstrates the nature of variations in intensity between relatively fine and relatively coarse sediments. There are algorithms which are sensitive to either the serial correlation of numerical values represented by such images, or the nature of texture within the images (i.e. 2D statistical properties which reveal something about the distribution of grey levels within an image). The numerical technique used processes a 2D image to produce a numerical signature of the spatial arrangement of image intensity.

Calibration images are taken of sediments which have been sieved into a number of size fractions, and the numerical procedure chosen is applied to each image to build up the catalogue (Fig. 2). The number of observations must equal the number of observations in the calibration catalogue, so the calibration catalogue will consist of n observations multiplied by m calibration sizes. The procedure then involves 'looking-up' the elements of the sample in the calibration catalogue and, based upon their location, returning output values interpolated within the

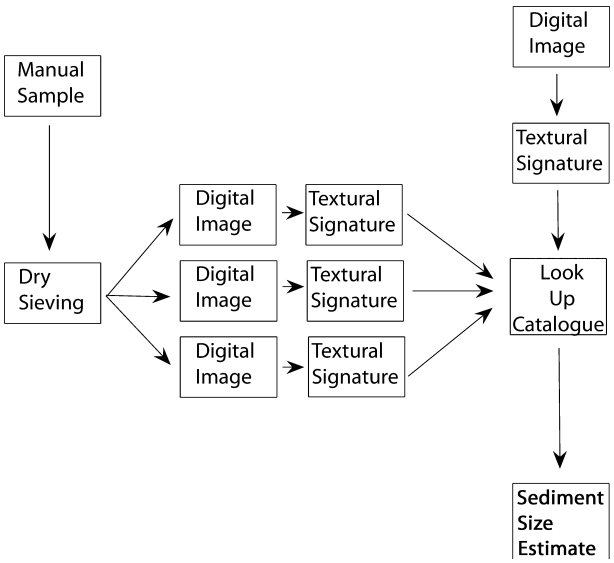

Fig. 2. Schematic diagram of the stages involved in the 'look-up cataloguing' procedure.

elements of the catalogue. The catalogue, therefore, is a 'look-up table' and this general procedure is termed here: 'look-up cataloguing' (LUC).

A digital image is then taken of each fraction, and a statistical procedure which is sensitive to the size of sediment on the greyscale complement of the image is then applied to the image. In this way, a calibration catalogue of numerical values for each sediment size is obtained. The collection of that image is crucial to the technique. In the field, images of sediment are taken and then analysed using the same statistical technique used previously to create the calibration catalogue (Fig. 2). Calibration and sample images have sufficient grains to have variation in colour and mineralogy, and images of grains have sufficient resolution so that the smallest grain in the image is larger than one pixel, to prevent aliasing problems. The largest grain-size likely to be encountered is smaller than the largest size catalogued by calibration to avoid numerical errors caused by linear extrapolation. Calibration ensures transferability to a range of sizes, shapes, lithologies and packing configurations, and is carried out whenever any of these changes significantly. The calibration is carried out again if the camera type or settings are changed, or if sediment sizes fall out of the range of the sizes used for calibration.

Estimating grain-size

The general linear equations for the problem of solving for the proportions of calibrated sizes that collectively give the best fit to the numerical signature of a given sample are modified from Rubin (2004):

$$\begin{aligned} &a_{(1,1)}x_1 + a_{(1,2)}x_2 + \cdots + a_{(1,m)}x_m = b_1 \\ &\vdots \\ &a_{(n,1)}x_1 + a_{(n,2)}x_2 + \cdots + a_{(n,m)}x_m = b_n \end{aligned} \quad (1)$$

where x_1 ,..., x_m are the proportion of size fraction 1:m in the sample; $a_{n,1}$,..., $a_{n,m}$ are the numerical signature values for lags 1:n of the calibration samples 1:m; and b_1 ,..., b_n are the observed numerical values for lags 1:n in the current sample. In matrix notation, this linear problem is therefore defined by:

$$a(n) = \sum_{k=1}^{m} C(n,k) \cdot X(n) \quad (2)$$

where a is the sample array (a column vector with n components) and C is the $m \cdot n$ calibration catalogue; where the vector solution $X = x_1{:}x_n$ is the one that minimizes the sum of squared errors between C and a, or $[a - \mathrm{C}^{\mathrm{T}}\, a - \mathrm{CX}]$; and where 'T' denotes matrix transpose. This solution is the array of grain-sizes generated from the image by effectively weighting proportions of several sizes. In this way, intermediate solutions which fall between two pre-computed values may be sought through interpolation. Solutions for sediments composed of mixed sizes are thus derived easily, for example, using a measure of central tendency (e.g. mean or median) of X.

Note that the linear problem described above is mathematically simple because there are as many equations as unknowns, and the solutions are always greater than zero, which collectively means that a solution is always found. The solution may be found in a least squares sense with or without constraints by minimizing [norm(aX − C)]. The simple matrix division of the sample array a into the calibration catalogue C [$aX = C$] may be computed through matrix methods such as Gaussian elimination (Gentle, 1998), where the solution X is again the array of sediment sizes (mm). However, use of the non-constrained approach is not recommended because derived coefficients may be positive or negative; thus it consistently underestimates the sediment size. Therefore, Rubin (2004) used an (iterative) optimization routine (Lawson & Hanson, 1974) to find the grain-size 'distribution', a vector solution which minimizes $[a - \mathrm{C}^{\mathrm{T}}\, a - \mathrm{CX}]$ such that $x > 0$ (i.e. a non-negativity constraint).

The Rubin (2004) size 'distribution' of length m, which assigns a proportional weighting to each size represented by the calibration, may yield an additional measure of grain-size, which is calculated as the sum of the product of each element of the distribution, d_1 ,..., d_n, and the corresponding size in millimetres, D_1 ,..., D_n:

$$D_{\mathrm{gsd}} = \sum_{i=1}^{n} d_i D_n \quad (3)$$

Trials have shown that, in practice, there is little difference between the size values found using the mean or median as size measures. This finding is because each value of the distribution represents the proportion of non-negative least squares variance, and the explained similarity attributable by the corresponding size fraction in the calibration catalogue; therefore, the size measure proposed above only accounts for the frequency of the size classes present in the

image, and not those absent. By contrast, the grain-size array X could contain negative elements, which is physically impossible. Ignoring the negative elements reduces the sample size yet further, which might be problematical for computations performed over relatively short lags, and will affect the accuracy of the estimated grain-size. Using the φ scale sieve mesh diameters in the gravel range for calibration, the larger the sediment the greater the potential errors caused by linearly interpolating over logarithmically spaced classes. Interpolating over linearly spaced size class intervals may introduce statistical artefacts because of the discontinuous (i.e. grouped) nature of the mass–frequency data.

NUMERICAL METHODS

The autocorrelation technique of Rubin (2004)

Positive spatial autocorrelation is the tendency for objects closer together to be more similar than objects further apart. Taking image intensity as a random (spatial) variable, the extent to which information within images is independent may be quantified using an autocorrelation function. If values separated by a lag of h are similar, the array will have an autocorrelation coefficient $r \rightarrow 1$, signifying serial dependence/correlation (Fig. 3), and if $r \rightarrow 0$ the sequence is random or serially uncorrelated. For images of natural beds, pixel patches covering larger grains are more similar for a longer distance than pixel patches covering smaller grains. Spatial autocorrelation as a function of incremental offset distance (lag) produces a (auto-)correlogram. Larger grains are therefore characterized by a shallow-slope correlogram and finer grains by a steep-slope correlogram (Fig. 3). Mean or median sediment size within the image is related strongly to correlogram slope, zero-crossing lag and given autocorrelation percentiles (Fig. 3).

The Rubin (2004) method for calculating the autocorrelation sequence performs better with one modification: a pre-processing step which rescales the image values to lie between 0 and 100 (rather than 0 and 255) and rounds these values to the nearest integer. This approach was found to enhance the differentiation between sizes by removing some short-wavelength noise in the images, thus removing the tendency for the correlogram to fluctuate around zero at larger offsets.

The autocorrelation function is a spatial operation; therefore, it is sensitive to non-square pixels, plus the direction through the image in which the algorithm is applied. Because of mixtures of sizes within the calibration images, differentiation of closely sized fractions of material can be difficult. At relatively large lags, the non-differentiation of individual correlograms introduces errors in the least squares solution, which often means that the calibration catalogue must be truncated at a relatively short lag (Barnard *et al.*, 2007; Rubin *et al.*, 2007).

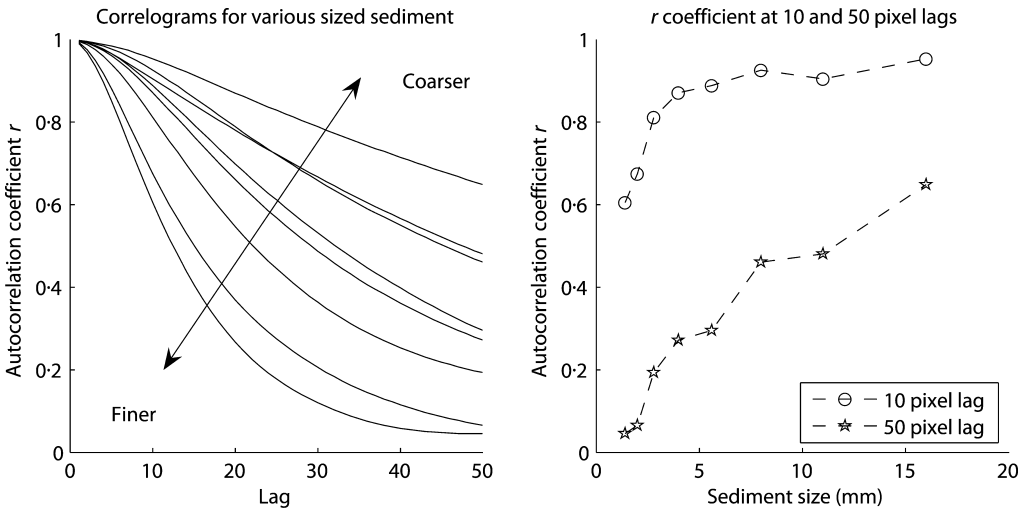

Fig. 3. The autocorrelation technique. Left: correlograms for various sized sediments. Right: r coefficients associated with the 10th and 50th lags of the correlogram, for different sediment sizes.

Better results may therefore be obtained in the frequency domain. Texture may be thought of as repetition of a basic structural pattern. In image processing, these repetitive basic elements are known as 'texels'. It has been shown that 'texture' may be quantified statistically by using frequency transforms (e.g. Tuceryan & Jain, 1998), which uncovers the nature and separation of repeating patterns and texture within that image, represented in a space whose coordinate system has an interpretation that is closely related to characteristics of texture. The contents of the entire image are mapped as energies at all frequencies and orientations; therefore, radial bins in the frequency domain detect and characterize both image texture directionality and the rapidity of fluctuation (Davis, 1986).

The Yule–Walker autoregressive model

Power spectral density (PSD) is estimated using the Yule–Walker method, which is closely related to autocorrelation but which operates in the frequency domain. Using a moving window, an autoregressive model is fitted to each successive portion of signal by minimizing errors associated with extrapolation (in a simple least squares sense; Priestly, 1994). The natural log transform of the PSD is sensitive to the size of grains in digital images (Fig. 4). The Yule–Walker equation can be expressed as:

$$\gamma_p = \sum_{k=1}^{p} \phi_k \gamma_{m-k} + \sigma_\varepsilon^2 + \delta_m \qquad (4)$$

where γ_m is the autocorrelation function of the input signal, φ_k are the autoregressive coefficients, σ_ϵ is the standard deviation of the input error (noise), δ_m is the Kronecker delta function, and $m = 0{:}p$, where p is the (user-defined) order of the model, at any point dictating how many previous values have an effect on the regression from the current window of values (Box & Jenkins, 1976). Because the last part of the equation is >0 only when $m = 0$, the Yule–Walker equation is usually solved as $p + 1$ simultaneous equations (Priestly, 1994).

The Yule–Walker model is used as a parametric spectral estimation method (solved using Levinson–Durbin recursion; Kay, 1988), instead of a periodogram (calculated using a Fourier transform, thus decomposing the data into a regular trigonometric series), because it produces a smoother power spectral density, and because order specification allows greater computational flexibility. In the present study, the order of the autoregressive model used for images of natural sediments is $P = 20$. The spectral density units are the squared magnitude of the frequency response of this model order (Kay, 1988).

Power spectral density for any given frequency will generally be higher for images of smaller sediment, because there is more variance associated with that frequency (Fig. 4). There is a strong

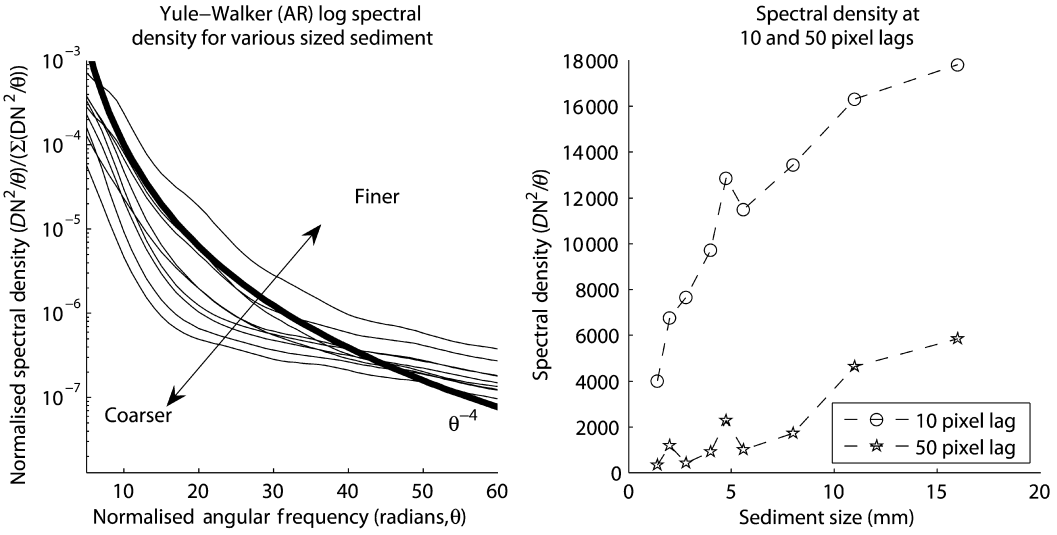

Fig. 4. The autoregressive (AR) PSD technique. Left: power spectral densities, in units of image intensity squared per normalized angular frequency in radians (θ, normalized so it sums to unity), for various sized sediments, calculated using an AR model (γ_p), order 20. The sediment takes the general form θ^{-4}, shown as a heavy line. Right: spectral density associated with the 10th and 50th frequencies, for different sediment sizes.

correlation between percentiles of power spectral slope and sediment size (Fig. 4). In the calibration catalogue, true exponential decay is achieved rather than fluctuations around zero when the spatial algorithm factors into the statistic patches of image intensity, which have been encountered before. The result is potentially a better differentiation of the curves in the catalogue.

2D Fourier transform

Operating in the non-spatial domain, each Fourier coefficient depends on all pixel locations, thus enhancing the computational efficiency (without compromising the validity) of traditionally spatial operations such as the calculation of the variogram. In images of natural sediments, textural patterns are scale-dependent phenomena. The type of Fourier transform applied on the images in this study is for an aperiodic, discrete signal, with a continuous spectrum.

Semi-variance is a measure of squared difference in intensity value between a pair of pixels located at a distance or lag. In the spatial domain, it is given by the classic equation (Davis, 1986):

$$\gamma(h) = \frac{E\{(x+h)_i, x_i\}^2}{2} \qquad (5)$$

where the numerator is the mathematical expectation E of the quadratic increments of pixel pair values separated by distance h, a vectorial function which varies with the modulus and angle of h between pixels $x + h$ and x (Gringarten & Deutsch, 2001). Image detrending is a necessary pre-operation. Semi-variance (γ) can be thought of as related to an inverse measure of spatial autocorrelation at a specified location vector, at a certain lag in a given direction. A plot of semi-variance as a function of lag distance is called a semi-variogram (Fig. 5). The semi-variogram has been used, for example, in the field of remote sensing to characterize textural properties of satellite imagery (e.g. Lark, 1996; Chica-Olmo & Abarca-Hernandez, 2000; Carbonneau *et al.*, 2004, 2005; Verdu *et al.*, 2005). The use of the semi-variogram on images of sediment is valid with respect to Tobler's Law (e.g. Kent *et al.*, 2006), because the correlogram is positive for all lag distances.

The variogram computation is performed using the algorithm detailed in Marcotte (1996) which uses a spectral, rather than spatial, domain approach. The complexity of operations is dictated by the number of pairs at all lags, n, given by $n = (2M - 1)(2N - 1) \cdot \log_2(2N - 1)$ for a Fourier transform approach, and $n = (NM)^2/2$ for a spatial approach, where $M \cdot N$ are the dimensions of the image. The frequency approach is simpler, in terms of operations, by a factor of $3{\cdot}4 \times 10^4$, with identical outputs.

The variogram of a 2D image using a spectral approach is defined by first defining a precursor γ_p:

$$\gamma_p = \left(\frac{\hat{F}_c F^* \hat{F} - 2F_c F}{n-2}\right) \qquad (6)$$

where $\hat{F}_c$ is the complex conjugate of $\hat{F}$ and F_c is the complex conjugate of F; where F, F^* and $\hat{F}$ are defined as the 2D Fourier transforms of x, x^2 and i,

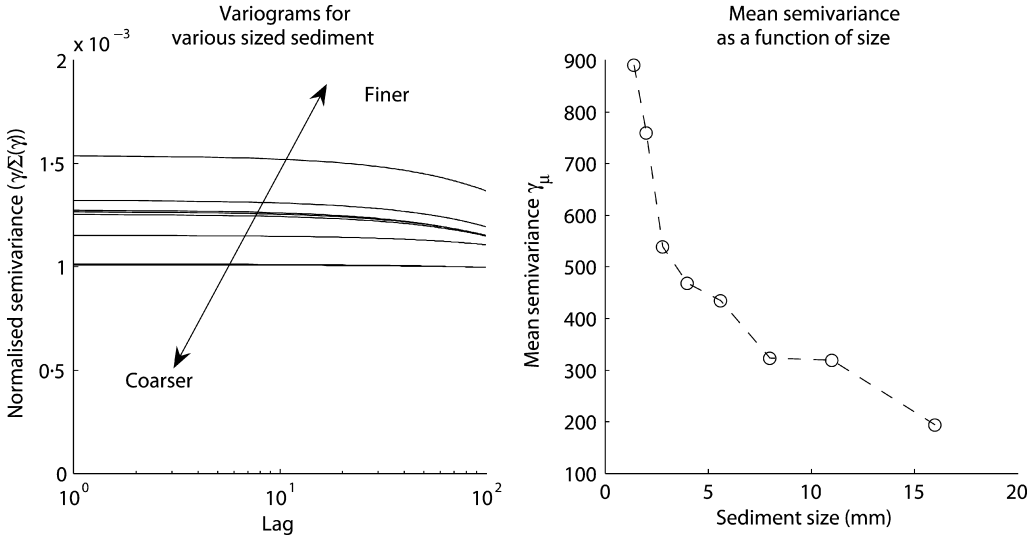

Fig. 5. The variogram technique. Left: semi-variance sequences for various sized sediments, normalized so they sum to unity. Right: mean semi-variance as a function of sediment size.

respectively; x is an image of dimensions (N, M); i is an indicator matrix of zeros of dimensions (N, M); and n is the number of pairs at all lags. The variogram γ is then given by the 2D inverse Fourier transform of γ_p, shifted so that the zero-frequency component is at the centre of the spectrum (Marcotte, 1996).

Images of larger grains have smaller mean semi-variance values for a given lag than images of relatively small grains (Fig. 5). Coarser sizes yield smaller semi-variance values because the light/shadow pattern is larger; therefore, the singularity fronts of the image, where the largest changes in intensity occur, are larger. Images of smaller sediments yield larger semi-variance values because the image intensities vary less as a vector function of lag than as a function of individual pixel values.

Fractal dimension

Some natural surfaces have (quasi-)linear log–log power spectra, in units of distribution of power per unit frequency. Images of natural sediments are such surfaces, and ordinary 2D-FT power spectral estimation, when a log–log (magnitude–frequency) transform is applied, is sensitive to the size of sediments within images (Fig. 6). The zero-frequency component of the image is shifted to the centre of the spectrum, and a 2D discrete Fourier transform is carried out on the detrended zero-shifted image. A linear least squares polynomial is fit to the data in the log–log plot of the phase magnitude and frequency, which finds the average slope (Fig. 6).

Voss (1988) demonstrated that, when spectral slopes are quasi-linear, the Hausdorff-Besicovitch, or fractal, dimension (D) can be calculated from the log–log transform of the image power spectrum. In such cases, the fractal dimension has been shown to be an appropriate spectral estimator of texture (Chaudhuri & Sarkar, 1995). The fractal dimension of the surface is given by 2 (the topological dimension of an image) plus the slope of a regression line through the data (Smith

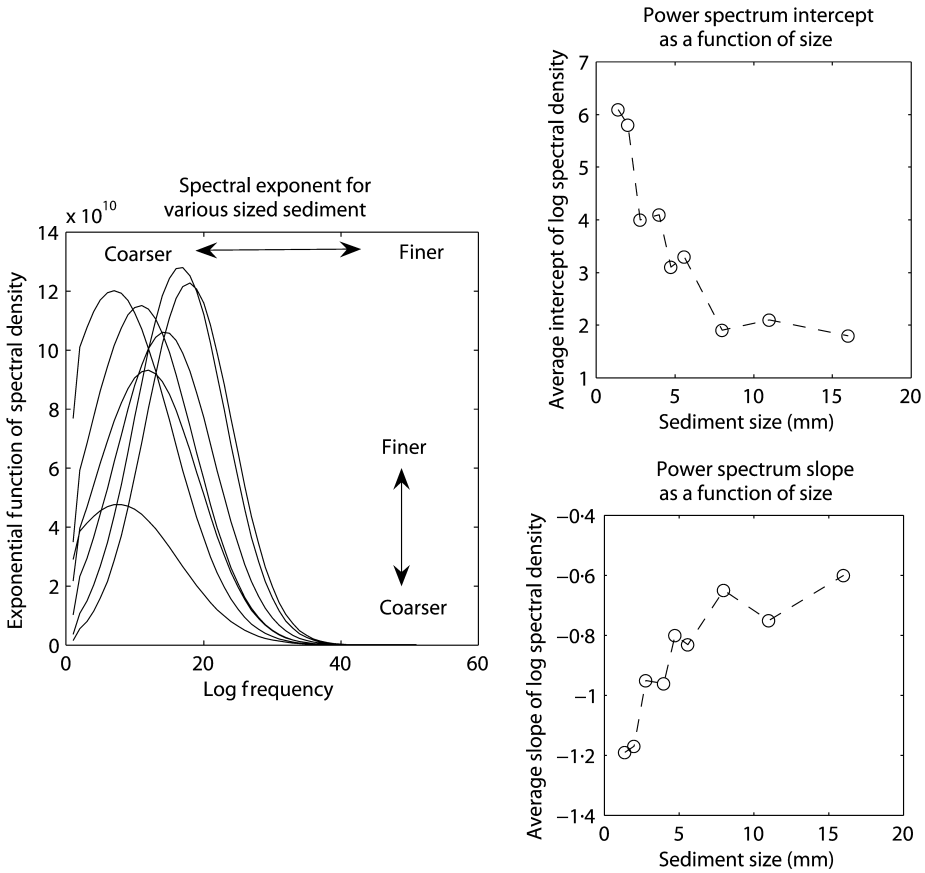

Fig. 6. Left: power spectral exponents for various sized sediments, in units of image intensity squared per normalized angular frequency in radians, derived using ordinary 2D-FT for various sediment sizes. Top right: mean log power spectral slope as a function of sediment size. Bottom right: log power spectral intercept as a function of sediment size.

et al., 1990; Bartlett, 1992). Plotting the log of the magnitude in all directions against the log of the corresponding frequency (Richardson plot: Mandelbrot, 1983) yields a linear relationship from which the fractal dimension is derived by the relationship:

$$D = 2 + \log(\Delta s/\Delta f) \quad (7)$$

where s is the spectral density and f is frequency (Whalley & Orford, 1989). The slope (always negative), fractal dimension (D), and intercept of the spectrum are all highly correlated with grain-size (Fig. 6). The larger the fractal dimension (D), the more variable or 'rugged' the grain surface, and the smaller the grain-size. Images of smaller grains have smaller scale invariance, or less self-similarity in image intensity through the image, than images of larger grains. Similar to PSD estimation using the Yule–Walker technique, images of smaller sediment have larger energy associated with smaller frequencies than images of larger sediment (Figs 4 and 6).

FIELD SITE AND IMAGE-COLLECTION METHODS

Field site

Slapton Sands in Devon, UK, is a 4·5 km long gravel barrier beach in Start Bay facing the English Channel to the east. The tidal regime is macrotidal and semidiurnal with spring and neap ranges of 4·3 and 1·8 m, respectively. The beach is steep, with intertidal slope tan β = 0·1, and composed of a range of sediment sizes between 1·4 and 50 mm, but with a median diameter D_{50} of approximately 6 mm, which is highly variable in space and time. Slapton often has distinct alongshore grading, which is typical of gravel beaches (e.g. Bird, 1996), yet the mechanisms of such grading, most famously seen at Chesil in Dorset, UK (e.g. Carr, 1971), are still debated, especially when the beaches are swash-dominated and morphological forms such as steps and berms are so coherent and consistent alongshore. It is, therefore, relevant to be able to map sediment size alongshore on such beaches as part of an investigation into the mechanisms which force spatial size grading. Slapton Sands also has distinct cross-shore grading of size, which changes on a much shorter timescale but is equally poorly documented, and largely unexplained.

Image collection for gravel-sized sediment

Generally, the more the calibration images, the better the size approximation; therefore, sieving at $\varphi/4$ and taking an image of each fraction is recommended. Samples for calibration in the gravel size range have been collected according to the recommendations of Church *et al.* (1987) and Gale & Hoare (1992) for coarse clastic sampling, where >2 kg of material is believed to be sufficient for well-sorted material up to 20 mm diameter, where the largest stone is <5% of the total mass.

For coarse sand and gravel beds, images are taken at a constant height above the surface. In the present study, this result was achieved by placing the camera in a housing at the top of a black box, which was open-ended and 50 cm tall. It was found that, as an axiom, images should be taken from a height in centimetres equal to the size of the largest grain measured in millimetres. The focal plane of the camera (Pentax® Optio S30 3·2 megapixel; PENTAX U.K. Ltd., Langley, Slough) was parallel to the object (surface) plane, and the settings of the camera were adjusted manually so that the focal plane was at the same distance above the ground as the camera lens (in some cameras an automatic adjustment may be made). The footprint of the image, in millimetres per pixel, may be found by:

$$p_{\mathrm{mm}} = 1/\left(\frac{r}{f/r^2}\right) \quad (8)$$

where f is the file size in bytes and r is the resolution in dots-per-inch (dpi). Using this formula, the image collection technique outlined above with a resolution of 0·0788 mm per pixel which is, in terms of pixels per millimetre, equivalent to 12·68 times the required resolution the size of grains under scrutiny (~1 to 20 mm).

A potential problem of poor (not constant) exterior lighting is overcome by incorporating lights into the camera housing (Rubin *et al.*, 2006, 2007; Barnard *et al.*, 2007). In the present study, sufficiently uniform lighting was provided by allowing the camera flash only to illuminate the bed (exterior lighting was removed by the camera box), so the technique was not sensitive to daylight and could be used both day and night. A constant illumination angle and magnitude

should be maintained by ensuring that the only light source is from the camera flash, thereby ensuring that shadows are at a constant angle and shading magnitude (hence information factored into the calibration catalogue), removing false intragrain edge noise and not biasing the statistic used. Items and markers need not be placed inside the image. The focal length of the camera was known, so the area represented by each image was also known, and this was held constant. Note that results are unaffected by variation caused by lens distortion, because the same distortion is within the calibration catalogue if the same camera and camera settings are used for both calibration and sampling. Images were inspected by eye for degree of exposure, or using a simple algorithm which flags images above and below thresholds of image noise associated with exposure problems.

Validation

A total of 181 samples were collected manually from various locations along Slapton, and two images taken of each before they were sieved into 17 classes in the $\varphi/4$ size range between 1 and 16 mm. The graphical (Folk and Ward) mean of each sample was compared with the 'distribution mean size' (Eq. 3) derived from images of those samples. The images (1536×2048 pixels, 100×130 mm) used in this study were collected using the methodology outlined above.

The results for the test area at Slapton are summarized in Fig. 7: close agreement is found by averaging over two images ($R^2 = 0{\cdot}82$–$0{\cdot}86$, mean absolute deviation less than 1 mm). The dashed lines indicate ±1 mm from the sieved sizes (solid line). Figure 7 shows that the majority of samples lay less than 1 mm from the solid line. Barnard *et al.* (2007) have shown recently that better size estimates are obtained if the size outputs from several images are averaged. In a similar vein, the present study managed to obtain a better size estimate by averaging over the values obtained from two different images and methods ($R^2 = 0{\cdot}88$–$0{\cdot}92$).

Accuracy was determined as the mean percentage deviation in imaged mean size from sieved

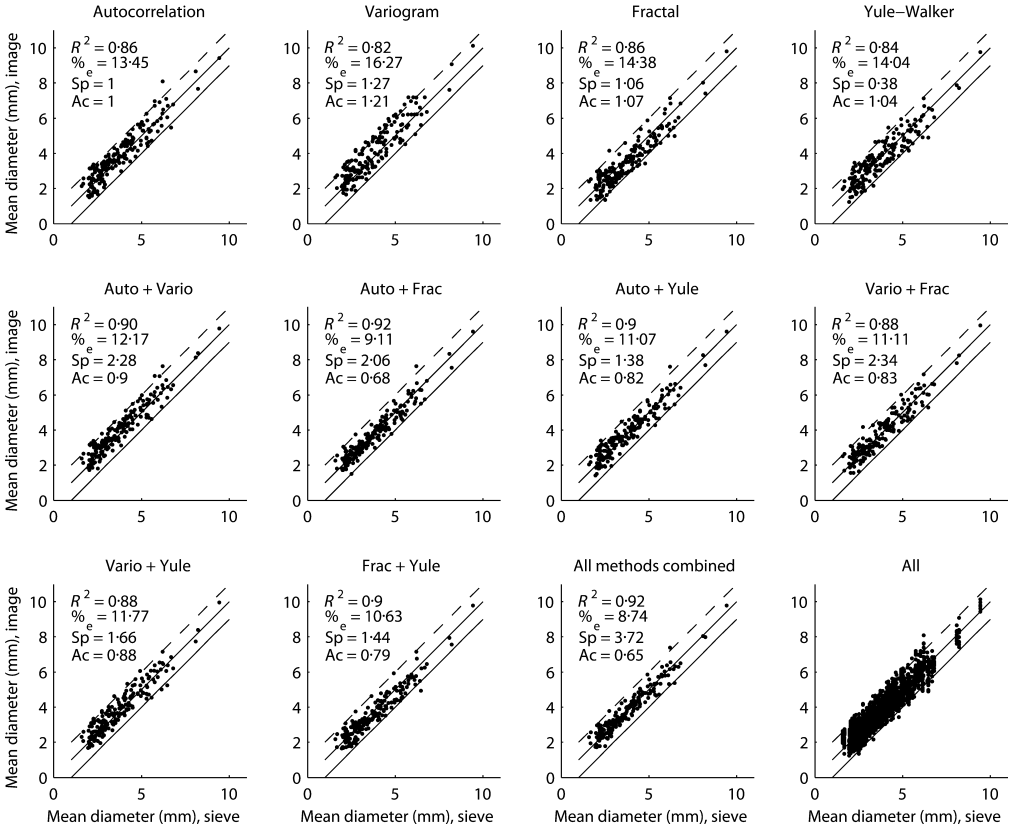

Fig. 7. Comparison between grain-size (mm) determined from 181 image samples and the graphical mean size (mm) determined by traditional sieving for that sample. Dashed line indicates a +1 mm departure in size. All values are Folk and Ward (1957) graphic mean.

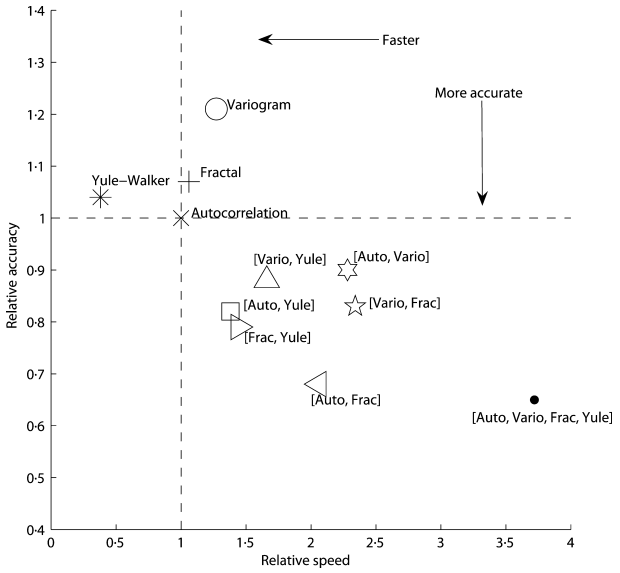

Fig. 8. A schematic summarizing the accuracy and speed of the techniques used in this study, based on 181 samples and relative to those obtained by the autocorrelation method. Speed increases right to left of the plot, and accuracy increases top to bottom.

mean size. The absolute processing time per sample was between 30 and 180 seconds. Relative accuracy was determined as the ratio of accuracy achieved by a given method (or combination of methods) to that achieved using the autocorrelation method. Similarly, relative speed was judged as the ratio of the time taken for a computation (using Matlab® version 7, with a >2 GHz dual processor; The MathWorks Inc., Novi, MI, USA) of a given method or combination of methods relative to the autocorrelation routine. Regression coefficients, accuracy, relative accuracy and relative speed for each technique are scribed into the top left of the sub-panels in Fig. 7. A schematic summarizing the trade-off between relative speed and relative accuracy for the methods used in this paper may be seen in Fig. 8.

Example applications

Images were taken along a grid at Slapton, measuring 30 × 40 m (Fig. 9). Mean surface sediment size was measured using a combination between size estimates obtained using the autocorrelation and Yule–Walker methods (74 images, ∼60 seconds per sample). The resulting surface shows that, although the beach section is very planar (top left), sediment size (top right) and associated parameters (bottom panels) vary considerably in space (Fig. 9).

Images were taken every ≈15 m along the 4·5 km length of Slapton along the high tide berm in January 2006, and again in June 2006, and sediment size calculated using the autocorrelation routine (∼600 samples, processing time ∼30 seconds per sample). Figure 10 shows the results of the surveys, which demonstrate that grading is much more pronounced in winter than in the summer, and that sediment size is generally coarser during the winter.

A cross-shore transect of images for sediment size, taken every 0·5 m from the previous high tide strand to the low tide shoreline (landward swash limit), was carried out every low tide (semi-diurnal spacing of ≈12·5 hours) for a whole spring–spring tidal cycle in late September 2005. Figure 11 shows the results of the surveys, using the fractal technique (∼2000 samples, processing time ∼40 seconds per sample). Sediment sizes are not displayed in real units because the cross-shore transects have been stacked to show the evolution of spatial trends through time. The 'master' median grain-size throughout the two-week period depicted here did not change, remaining at ≈7 mm, but there was large spatial segregation of the fine (<7 mm) and coarse (>7 mm) fractions through time. The left panel of Fig. 11 shows the evolution of sediment size during the first week (spring to neap, up the page), and the right panel shows the second week (neap to spring, up the page). Two modes of behaviour were observed: coarsening seawards, and fining seawards (these cross-shore transects are denoted in Fig. 11 by thicker black lines). Over the two-week period there was considerable switching between these two behaviours. Under neap tide there was more time on the falling tide for sediments to sort into collections of size, making spatial gradients in sediment size more pronounced.

DISCUSSION

Rubin (2004) showed that the autocorrelation function, used as a measure of 2D spatial dependence, could be sensitive to the size of grains within images of sand and thus, given calibration, could be used to derive a rapid, yet accurate, measure of sediment size. This development makes it possible to use digital imagery to measure grain-size in almost real-time in the field and in the laboratory, enabling significant improvements in spatial and temporal coverage and

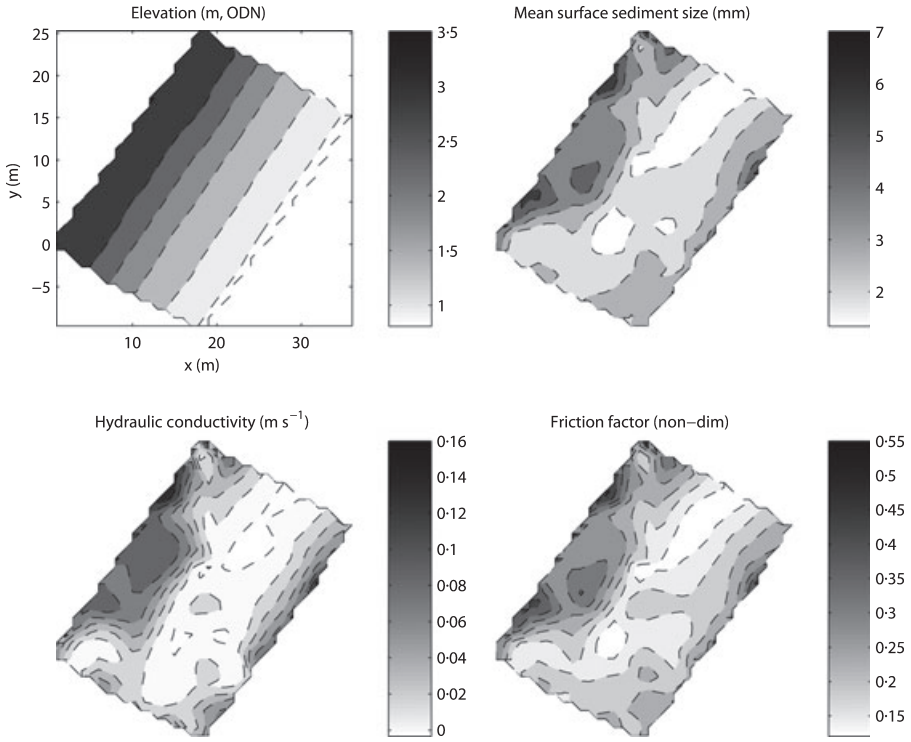

Fig. 9. A 30 × 40 m area section of beach at Slapton Sands, UK. Top left: elevation (m, ODN). Top right: mean imaged surface sediment size (mm). Bottom right: friction factor (non-dimensional, a descriptor of bed roughness) calculated using the method of Swart (1974) for 10 sec period and 1 m significant wave height. Bottom left: hydraulic conductivity (cm s^{-1}).

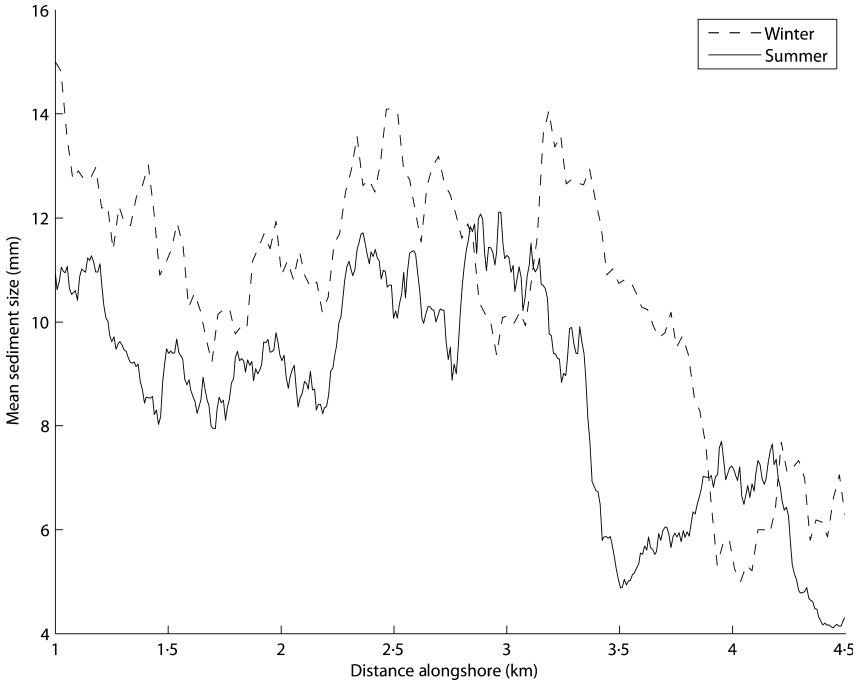

Fig. 10. Sediment size as a function of distance alongshore at Slapton Sands, Devon, UK. Dashed line indicates winter profile and solid line indicates summer.

resolution (Rubin *et al.*, 2006, 2007; Barnard *et al.*, 2007; Ruggiero *et al.*, 2007). Automation of the sampling and analysis process should elucidate subtle grain-size response at high temporal and spatial resolution, highlighting, for example, the close kinematic coupling between

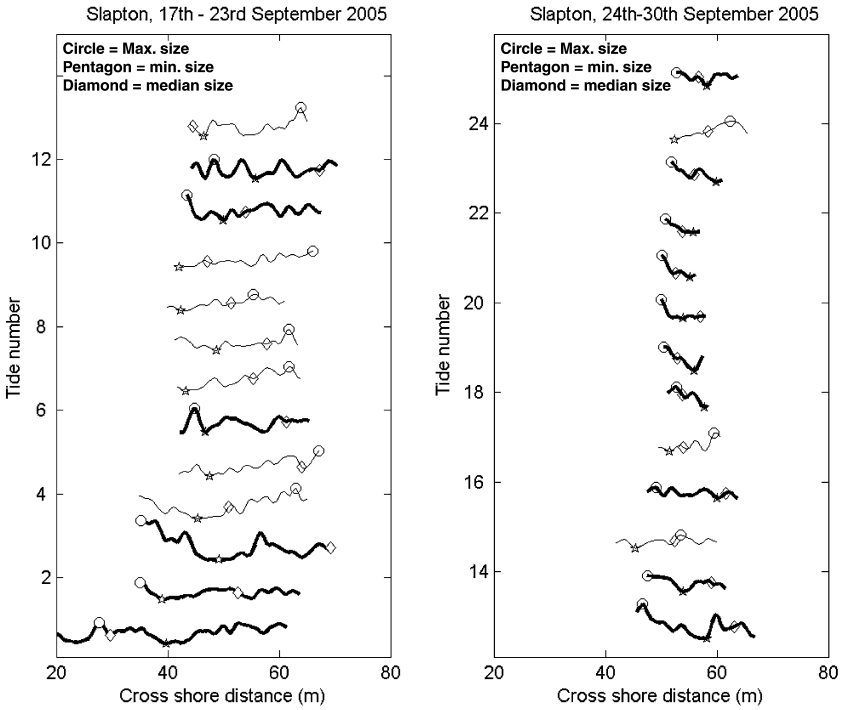

Fig. 11. Sediment size along a cross-shore beach transect in the centre of Slapton Sands, for 26 consecutive tides between 17 and 30 September 2005. Note that absolute sediment sizes are not shown to facilitate timestacking, i.e. sediment sizes are not displayed in real units because the cross-shore transects have been stacked to show the evolution of spatial trends through time. The general variations can be seen, as well as the positions of maximum (circles), median (diamonds) and minimum (stars) sizes.

bed composition and flow fields (e.g. Rubin & Topping, 2001; Gallagher *et al.*, 2006). The resultant availability of high-resolution grain-size distributions, time-varying grain-size, and derived parameters such as porosity, may lead to the development of new sediment transport and morphological models because shear stresses, friction and transport efficiency terms will be updated with reference to grain-size more efficiently.

In autoregressive methods, the choice of lag numbers/model order is crucial: a small number ignores large lag correlations, and a large number leads to loss of power at smaller frequencies. The optimal lag for beach gravels was $h = 20$ for the autoregressive (AR) model (γ_p), and >50 for the autocorrelation method, although these recommendations may change for different sedimentary environments. The advantage of 2D-FT methods is that the number of lags (or order number) does not need to be specified, thus saving time and effort in numerical trials at the calibration stage. Furthermore, spectral techniques map image components of all frequencies, and high power in low frequencies (Ojala *et al.*, 1996) should enable this class of technique to characterize processes with long periodicities (e.g. very large grains, or features in coarse resolution images better, which would require several lags using an autoregressive routine). The autocorrelation technique is relatively inflexible. Spectral techniques are more flexible because of inherent directionality, and the Yule–Walker AR technique has flexibility in operator-defined model order. This advantage of autoregressive models may be beneficial in, for example, quantifying different sized sediments, mixed sediments, or different image collection procedures.

In addition to the four techniques mentioned here, there are a number of others which may be suitable, including Portmanteau sequences, multifractals and wavelets (cf. Rubin, 2004). Further work is required to differentiate better between grain-sizes in poorly sorted mixtures when using power spectral techniques, and also to characterize the statistical properties of sediment images for use in determination of other geometrical characteristics such as sorting which, most importantly, requires more work to approximate the entire grain-size distribution better, rather than just mean size.

The new methods outlined here may facilitate the generation of artificial sediment surfaces for use in sedimentary modelling (e.g. Hardy, 2005). For example, it may be possible to simulate grain surfaces using fractal terrain simulators (e.g. Outcalt & Melton, 1992) or theoretical forms of the variogram. To this end, and by way of example, it was found that digital images of natural sediments corresponded well with a circular model (Gringarten & Deutsch, 2001) which is given by:

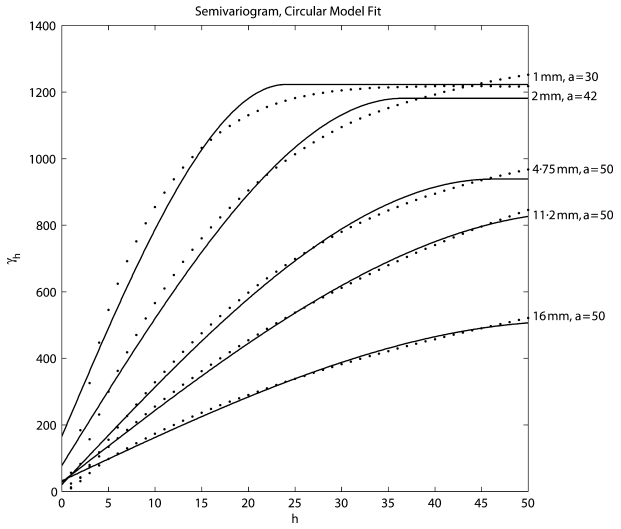

Fig. 12. A theoretical circular model (solid lines) fitted to empirical semi-variograms derived from digital images of various sized sediments (black markers).

$$\gamma_c = \begin{cases} C_0 + C \cdot 1.5(h/a) - 0.5(h/a)^3 & 0 \leq h \leq a \\ 0 & h = 0 \\ C_0 + C & \text{otherwise} \end{cases} \quad (9)$$

where a is a tuning parameter required for model fit. Figure 12 shows circular model fit (and associated values of a) to the empirical spatial semi-variograms for different sized images of sediment (calibration images for 1, 2, 4·75, 11·2 and 16 mm sediment). Note that for relatively large sediment (>4 mm), the circular model is cubic (i.e. the second term $[h/a]^3$ becomes dominant) where $[h/a] \approx 1$. In contrast, for relatively fine sediment (<4 mm), the two terms (linear and cubic) are equally dominant because $[h/a] \neq 1$, meaning a composite linear least squares fit is required.

Currently, the major disadvantage of an LUC approach to grain-size from digital images is that it is not transferable between sites unless a calibration is performed which accounts for potentially significant variations in size range, colour/mineralogy, etc. The techniques outlined in this paper potentially allow the quicker construction of a more robust calibration catalogue when so desired. Thresholding segmentation techniques will still be an attractive option for sedimentologists working in areas where repeat surveying is not required, and/or where few samples (<∼100) from that environment are needed.

However, a key point is that unless a threshold segmentation method perfectly identifies the perimeters of each individual grain, it will disaggregate some and aggregate others. Measures of mean/median size from the resulting size-mass distribution are still a function of the random false aggregation or disaggregation of grains within the image but, if the effects of aggregation and disaggregation are equal, the mean size is a good approximation of the truth. Segmentation thresholding techniques currently work less well for sand-sized sediment as opposed to gravel, perhaps because grain aggregation becomes more common than disaggregation, thus mean/median sizes usually are overestimates. The fact that images of natural sediment beds have fractal scaling is a potentially important finding for developments in segmentation thresholding of individual grains. The sum length of perimeter in an image of natural grains is related to some power of the average area (that power being the fractal dimension of the grain), so relatively small reductions in area cause disproportionately large increases in sum perimeter length. That the length of perimeter which must be successfully segmented in an image of natural grains increases as some power of grain area (thus diameter holding shape constant), and because current thresholding techniques are not perfect, collectively mean that the number of misidentifications increases disproportionately with reducing grain-size. The above implies that there may be some practical lower limits to the size of material successfully identified by application of segmentation threshold methods, and that lower limit is considerably higher than that currently used for a LUC approach.

It is important to remember that grain-size derived from sieving and from a LUC method are unlikely to be equivalent because of the 2D nature of the image, so better calibrations may be made by point counts of grain in images (e.g. Barnard *et al.*, 2007). A test was performed to see whether the fractal nature of images is dependent on the method employed to calculate the fractal dimension (D). Remembering that D is inversely proportional to sediment size (in mm), it was suspected that fractal dimensions found for coarser sediments using 2D-FT were overestimated (larger) because of the hiding of portions of the larger grains within the three-dimensional (3D) fabric of the sediment bed, both within mixed beds and calibration images, using the 2D-FT method. This effect causes larger sediments to plot in fractal space as finer than they are in reality. Using this method, coarser sediments have shallower slopes: spectral densities

associated with coarser sediments are therefore either higher at low frequencies, or lower at high frequencies, than they ought to be. This result may be because spectral densities are measured in units of squared intensity, whereas in reality the importance of absolute intensity magnitude is of subordinate relevance to relative intensity magnitude across local space as a function of frequency. In addition, spectra contain directional information which may complicate the estimation of fractal dimension. Therefore, a fractal estimation technique was sought which is less sensitive to absolute magnitude of image intensity at varying frequencies, more sensitive to the general shape of the intensity trace through images of sediment, and non-directional.

The classic approach is to calculate D by chord-fitting by measuring the length of data with different sized chords, based on the notion that the distance measured will depend on the size of the chord used (Mandelbrot, 1983). This approach may be expressed as:

$$D = \frac{\log N}{\log(1/R)} \tag{10}$$

where N is the number of times a measurement is taken (or the number of 'rulers' used) and R is the length of chord used to measure the distance (or the ruler length). Morphological opening, using structure functions (kernel operators) of differing lengths, was applied to images representing different-sized sediments. A linear structure function applied to an image preserves regions which have a similar shape to that function, while destroying regions which do not (Radhakrishnan & Dinesh, 2006). As the length of that function increases, less image detail is preserved after the operation. Figure 13 shows the progressive loss of detail (smoothing) when structure functions of increasing length (5, 50 and 100 pixels) are applied to an image of 1·4 mm sediment. The details of the sediment are progressively missed, tantamount to removing objects from the data stream, and analogous to the

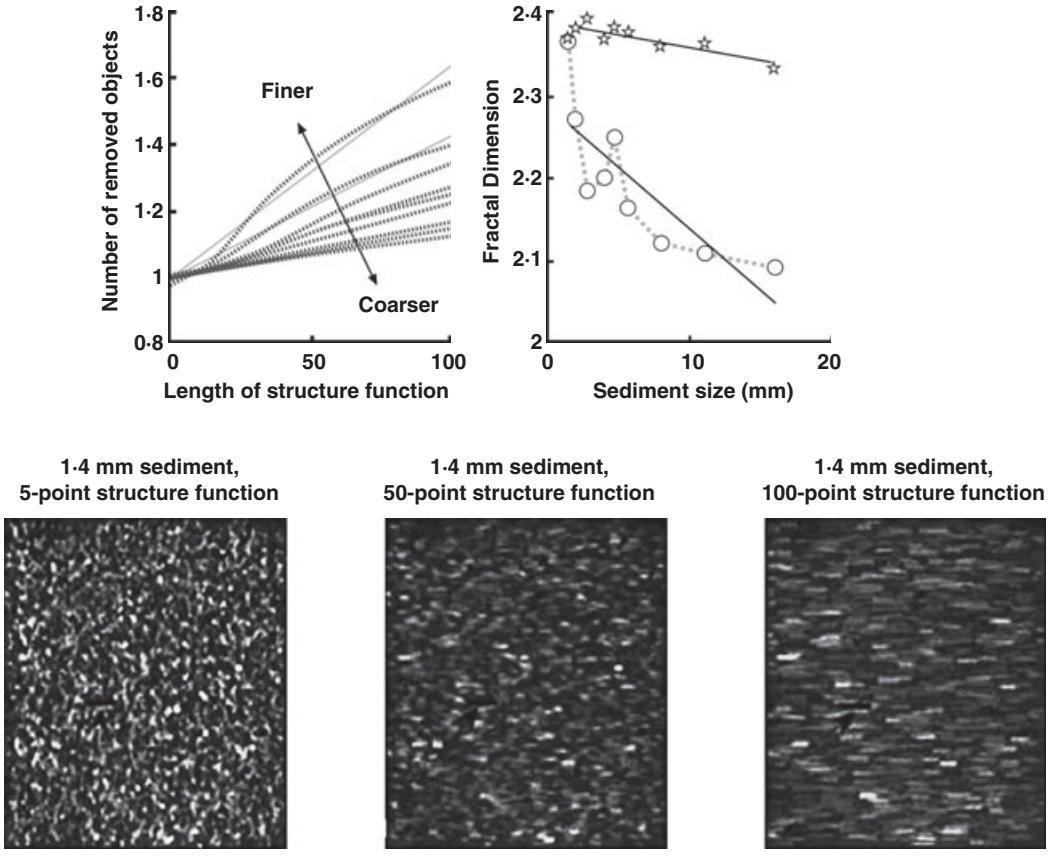

Fig. 13. The fractal nature of images of sediment. Top left: associated loss of detail in the resulting intensity trace, and the relationship between structure function length and loss of detail for various sized sediments. Top right: comparison between fractal dimensions estimated using the 2D-FT and chord-fitting methods. Bottom panels, from left to right: 1·4 mm sediment after application of morphological opening operations (5, 50 and 100 pixel linear structure functions).

lengthening of the ruler. Figure 13 shows this effect on a short (400 pixel) section of data, with the same 5, 50 and 100 pixel structure functions. Sections of images of finer sediment contain more detail than corresponding sections of images of coarser sediments. The effect of removing objects by morphological opening is therefore a function of sediment size within the image (Fig. 13). In other words, there is an inverse relationship between sediment size and slope of the number of objects removed with increasing structure function length. This relationship occurs because coarser sediments are more similar for a longer distance, therefore, there are more pixel regions of similar shape to that function, and so increasing structure function length removes fewer objects (Fig. 13).

Fractal dimensions for this linear relationship were obtained by dividing the slope of the natural logarithm regression line through the data (log N) by the reciprocal of the log ratio between the original image and the image after application of 100 structure functions of increasing length ($1/R$). These images are shown in Fig. 13 and provide circumstantial support to the notion that fractal dimensions calculated using a 2D-FT method, while still showing the inverse trend with sediment size consistent with theory, are overestimated. It may be the reason why differentiation of sediment size on a log–log power spectral frequency plot is more difficult. The use of the classic chord-fitting approach is intuitive in a fractal sense because as detail is successively removed, data length must decrease as the ruler size increases, therefore, very coarse sediments, which are more similar for a longer distance, must have a fractal dimension with a much smaller increment.

CONCLUSIONS

This study extends the image-collection methodology proposed by Rubin (2004) and Rubin *et al.* (2006, 2007) for sand-sized sediments to larger sediment sizes, thus grain-sizing from images is now possible in the full range from fine sands to medium gravels. Several new methods for digital grain-size estimation are proposed, and their relative merits discussed. The Rubin (2004) method performed better with a modification to enhance the differentiation between sizes by removing some short wavelength noise in the images, thus removing the tendency for the correlogram to fluctuate around zero at larger offsets. The Fourier analysis of an image can detect and characterize image texture directionality, which may have implications in later studies for quantifying sediment shape and orientation. The power spectral density of a digital image of sediment takes the general form θ^{-4}, where θ is normalized angular frequency in radians. The fractal dimension of an image is a sensitive indicator of the size of particles in that image. Fractal dimensions found for coarser sediments using two-dimensional (fast) Fourier transform (2D-FT) were overestimated perhaps because of the hiding of portions of the larger grains within the fabric of the sediment bed. A classic chord-fitting approach using morphological structure functions was more suitable. The fractal scaling of images of natural sediment beds may impose a practical lower limit on digital grain-size analysis using segmentation thresholding methods. Digital images of natural sediments corresponded well with a spherical semi-variogram model. For relatively large sediment (>4 mm), the circular model is cubic and for relatively fine sediment (<4 mm), a composite linear least squares fit is required. The primary appeal of the methods described in this paper is the speed at which several sediment samples may be processed for derivation of mean/median size. The trade-off between the accuracy obtained and the speed with which samples are estimated, using different methods or a combination of methods, is addressed. Based on over 180 samples, mean grain-size of sieved and imaged sediments corresponded to within between 8% and 16%. Better size estimates are achieved by averaging over the values obtained from two or more methods and/or images.

ACKNOWLEDGEMENTS

This manuscript was improved by reviewers: Dr Edith Gallagher, Dr David Rubin, Dr Patrice Carbonneau and an anonymous referee, to whom we are very grateful. Special thanks are also due to editors Prof. Paul Carling and Dr Susan Marriott. Thanks are due to Dr Rana Moyeed for a helpful discussion regarding variogram calculation; and to Slapton Ley Field Studies Council for their continuing logistical support. Finally, a big thank you to field assistants Amaia Alegria, Josh Gibson, Tom Deacon, Isabelle Emmanuel and Tamsin Watt for their help with data collection. DB acknowledges receipt of a UoP S.S.B Faculty Scholarship. Matlab® code for all methods

described in this paper is available from the authors.

REFERENCES

Austin, M. J. and **Bullard, J.** (2007) Variation and distribution of sediments in a mixed glacifluvial-aeolian system in West Greenland. *Eos Trans. AGU*, **88,** Fall Meet. Suppl., Abstract H54E-03

Barnard, P.L., Rubin, D.M., Harney, J. and **Mustain, N.** (2007) Field test comparison of an autocorrelation technique for determining grain-size using a digital 'beachball' camera versus traditional methods. *Sed. Geol.*, **201,** 180–195.

Bartlett, M.L. (1992) Comparison of methods for measuring fractal dimensions. *Austr. Phys. Eng. Sci. Med.*, **14,** 146–152.

Bird, E.C.F. (1996) Lateral grading of beach sediments: a commentary. *J. Coastal Res.*, **12,** 774–785.

Box, G.E.P. and **Jenkins, F.M.** (1976) *Time Series Analysis: Forecasting and Control*, 2nd edn. Holden-Day, San Francisco, CA, 592 p.

Butler, J.B., Lane, S.N. and **Chandler, J.H.** (2001) Automated extraction of grain-size data from gravel surfaces using digital image processing. *J. Hydraul. Res.*, **39,** 519–529.

Carbonneau, P.E., Lane, S.N. and **Bergeron, N.E.** (2004) Catchment-scale mapping of surface grain-size in gravel bed rivers using airborne digital imagery. *Water Resour. Res.*, **40,** W07202.

Carbonneau, P.E., Bergeron, N.E. and **Lane, S.N.** (2005) Automated grain-size measurements from airborne remote sensing for long profile measurements of fluvial grain-sizes. *Water Resour. Res.*, **41,** W11426.

Carr, A.P. (1971) Experiments on longshore transport and sorting of pebbles: Chesil Beach, England. *J. Sed. Petrol.*, **41,** 1084–1104.

Chaudhuri, B. and **Sarkar, N.** (1995) Texture segmentation using fractal dimension. *IEEE Trans Pattern Anal. Machine Intelligence*, **17,** 72–77.

Chica-Olmo, M. and **Abarca-Hernandez, F.** (2000) Computing geostatistical image texture for remotely sensed data classification. *Comput. Geosci.*, **26,** 373–383.

Church, M.A., McLean, D.G. and **Wolcott, J.F.** (1987) River bed gravels: sampling and analysis. In: *Sediment Transport in Gravel Bed Rivers* (Eds C.R. Thorne, J.C. Bathurst and R.D. Hey), p. 43–87. John Wiley, London.

Davis, J.C. (1986) *Statistics and Data Analysis in Geology*, 2nd edn. . John Wiley, New York, 656 p.

Gale, S.J. and **Hoare, P.G.** (1992) Bulk sampling and coarse clastic sediments for particle size analysis. *Earth Surf. Proc. Land.*, **17,** 729–734.

Gallagher, E., MacMahan, J., Russell, P., Masselink, G. and **Auger, N.** (2006) Grain-size from digital images and morphological variability. 30th Int. Conf. Coastal Eng., San Diego, CA, USA.

Gentle, J.E. (1998) *Numerical Linear Algebra for Application in Statistics*. Springer-Verlag, Berlin, 221 p.

Graham, D.J., Rice, S.P. and **Reid, I.** (2005) A transferable method for the automated grain sizing of river gravels. *Water Resour. Res.*, **41,** W07020. doi:10.1029/2004WR003868.

Gringarten, E. and **Deutsch, C.V.** (2001) Variogram interpretation and modeling. *Math. Geol.*, **33,** 507–534.

Hardy, R.J. (2005) Modelling granular sediment transport over water-worked gravels. *Earth Surf. Proc. Land.*, **30,** 1069–1076.

Kay, S.M. (1988) *Modern Spectral Estimation: Theory and Application*. Prentice Hall, Upper Saddle River, NJ, USA, 576 p.

Kent, M., Moyeed, R.A., Reid, C.L., Pakeman, R. and **Weaver, R.** (2006) Geostatistics, spatial rate of change analysis and boundary detection in plant ecology and biogeography. *Prog. Phys. Geogr.*, **30,** 201–231.

Lark, R.M. (1996) Geostatistical description of texture on an aerial photograph for discriminating classes of land cover. *Int. J. Remote Sens.*, **15,** 2437–2450.

Lawson, C.L. and **Hanson, R.J.** (1974) *Solving Least Squares Problems*. Prentice-Hall, Upper Saddle River, NJ, USA. 350 p.

Mandelbrot, B.B. (1983) *The Fractal Geometry of Nature*. W.H. Freeman and Co., New York, 468 p.

Marcotte, D. (1996) Fast Variogram Computation with FFT. *Comput. Geosci.*, **22,** 1175–1186.

Ojala, T., Pietikainen, M. and **Harwood, D.** (1996) A comparative study of texture measures with classification based on feature distributions. *Pattern Recogn.*, **29,** 51–59.

Outcalt, S.I. and **Melton, M.A.** (1992) Geomorphic application of the Hausdorff-Besicovich dimension. *Earth Surf. Proc. Land.*, **17,** 775–787.

Priestly, M.B. (1994) *Spectral Analysis and Time Series*. Academic Press, London, 890 p.

Radhakrishnan, P. and **Dinesh, S.** (2006) An alternative approach to characterize time series data: case study on Malaysian rainfall data. *Chaos, Solitons and Fractals*, **27,** 511–518.

Rubin, D.M. (2004) A simple autocorrelation algorithm for determining grain-size from digital images of sediment. *J. Sed. Res.*, **74,** 160–165.

Rubin, D.M. and **Topping, D.** (2001) Quantifying the relative importance of flow regulation and grain-size regulation of suspended sediment transport (alpha) and tracking changes in grain-size of bed sediment (beta). *Water Resour. Res.*, **37,** 133–146.

Rubin, D.M., Chezar, H., Harney, J.N., Topping, D.J., Melis, T.S. and **Sherwood, C.R.** (2006) Underwater microscope for measuring spatial and temporal changes in bed-sediment grain-size. USGS Open File Report 2006-1360.

Rubin, D.M., Chezar, H., Harney, J.N., Topping, D.J., Melis, T.S. and **Sherwood, C.R.** (2007) Underwater microscope for measuring spatial and temporal changes in bed-sediment grain-size. *Sed. Geol.*, **202,** 402–408.

Ruggiero, P., Adams, P.N. and **Warrick, J. A.** (2007) Mixed sediment beach processes: Kachemak Bay, Alaska. *Proc. Coastal Sediments*, **1,** 463–476.

Sime, L.C. and **Ferguson, R.I.** (2003) Information on grain-sizes in gravel bed rivers by automated image analysis. *J. Sed. Res.*, **73,** 630–636.

Smith, T.G., Marks, W.B., Lange, G.D., Sheriff, W.H. and **Neale, C.A.** (1990) A fractal analysis of cell images. *J. Neuroscience Methods*, **27,** 173–180.

Swart, D.H. (1974) Offshore sediment transport and equilibrium beach profiles. Delft Hydraulics Laboratory Publication 131.

Tuceryan, M. and **Jain, A.K.** (1998) Texture Analysis. In: *The Handbook of Pattern Recognition and Computer Vision*, 2nd edn (Eds C.H. Chen, L.F. Pau and P.S.P. Wand), pp. 207–248. World Scientific Publishing Co, Hackensack, NJ, USA, 652 p.

Verdu, J.M, Batalla, R.J. and **Martinez-Casasnovas, J.A** (2005) High-resolution grain-size characterisation of gravel bars

using imagery analysis and geo-statistics. *Geomorphology*, **72,** 73–93.

Voss, R.F. (1988) Fractals in nature. In: *The Science of Fractal Images* (Eds H.O. Peitgen and D. Saupe), pp. 21–70. Springer-Verlag, New York.

Whalley, W.B. and **Orford, J.D.** (1989) The use of fractals and pseudofractals in the analysis of two-dimensional outlines: review and further exploration. *Comput. Geosci.*, **15,** 185–197.

Manuscript received 26 March 2008; revision accepted 25 April 2008